

# Combining Chemical Functionalization and FinFET Geometry for Field Effect Sensors as Accessible Technology to Optimize pH Sensing

Dipti Rani <sup>1</sup>, Serena Rollo <sup>1,2</sup>, Wouter Olthuis <sup>2</sup>, Sivashankar Krishnamoorthy <sup>1</sup> and César Pascual García <sup>1,\*</sup>

<sup>1</sup> Nano-Enabled Medicine and Cosmetics Group, Materials Research and Technology Department, Luxembourg Institute of Science and Technology (LIST), Belvaux L-4422, Luxembourg; dipti.rani@list.lu (D.R.); serena.rollo@list.lu (S.R.); sivashankar.krishnamoorthy@list.lu (S.K.)

<sup>2</sup> BIOS Lab on Chip Group, MESA+ Institute for Nanotechnology, University of Twente, 7522 NB Enschede, The Netherlands; w.olthuis@utwente.nl

\* Correspondence: cesar.pascual@list.lu; Tel.: +352-275-888-583

## 1. Fitting for Determination of Thickness and Refractive Index of APTES Layer on SPR Sensor Chips using LayerSolver Software

The thickness ( $d$ ) and refractive index ( $n$ ) of the material/layer on the SPR chip are evaluated from the shape and quantities associated with the SPR curve. Fresnel's equations as the reflectivity of a system with multiple layers for a p-polarized light were used to fit the SPR spectra. In the LayerSolver software numerical iterations are carried out by embedded algorithms. The equations used for calculation routines are briefly described here [1] and require the existence of at least one layer with complex refractive index given as  $n = n + ik$  with the real part ( $n$ ) which corresponds to the refraction of light and the complex coefficient  $k$  that defines the extinction or absorption of light by material (or layer). For practical experiments it is assumed that the surface plasmon wave vector ( $k_{sp}$ ) contains all the information and constants which cause the differences in the measured SPR spectra at different wavelengths or in different media. The SPR spectra acquired in one set of conditions is not accurate enough to determine the differences in  $n$  and  $k$  accurately and hence only a continuum solution for  $k_{sp}$  vector proportional to  $n$  and  $d$  is deducted [1]:

$$k_{sp} \propto n * d \quad (1)$$

To evaluate a unique solution for the interconnected  $n$  and  $d$  of the layer added on the SPR chip, a measurement in two different media or at multiple wavelengths is needed. For measurements taken at two different wavelengths, unique solution for  $n$  (wavelength dependent) and  $d$  can be evaluated by solving the following equations:

$$k_{sp1} \propto n_{\lambda 1} * d \quad (2)$$

$$k_{sp2} \propto n_{\lambda 2} * d \quad (3)$$

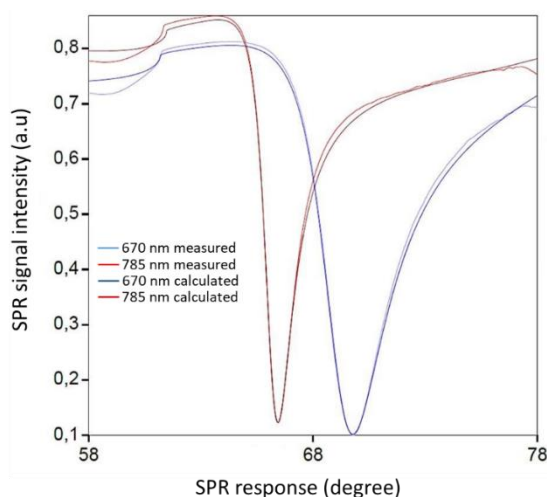


**Figure S1.** Full SPR spectra after APTES silanization of the SPR sensor chips at two wavelengths, 670 and 785 nm, illustrating good alignment between the measured and the modeled data. The measured spectra are shown in light blue and red colors while the modeled one as dark blue and brown colors.

Where  $k_{sp1}$ ,  $n_{\lambda1}$  denote the surface plasmon vector and refractive index for wavelength 1 ( $\lambda_1$ ), while  $k_{sp2}$ ,  $n_{\lambda2}$  represent the surface plasmon vector and refractive index for wavelength 2 ( $\lambda_2$ ). For layers which absorb light, a unique solution is given for the sample layer in the  $k_{sp} = (n+ik)*d$  space and two wavelengths are used to irradiate simultaneously the same spot at the layer deposited on the SPR chip.

The Layersolver software uses a model that includes the optical constants ( $n$ ,  $k$ ) and thicknesses of the different layers in the sensor chip: Cr, Au and SiO<sub>2</sub>. The fitting routines were launched with the nominal parameters from the chip provider, and then they were fit to the full angle reflectogram obtained with both wavelengths from the original chip. The thickness of the layers to be optimized (e.g., Cr, Au, SiO<sub>2</sub>) in the model was set as dependent variable for the two wavelengths while optical constants were set as independent variables. Different iterations were carried out to fit the model data to the measured SPR curve prior to APTES functionalization obtaining layer thickness of 3, 50 and 10 nm for the Cr, Au and SiO<sub>2</sub>, respectively. These values were kept fixed and a new process was then run after APTES functionalisation leaving the refractive index as independent and the thickness of the APTES layer as dependent variables for the fitting of the two wavelength reflectograms. Figure SI 1 shows the measured and the modeled SPR spectra for the APTES functionalized sensor chips at two wavelengths, 670 and 785 nm. The measured spectra are represented in light blue and red colors while the modeled one in dark blue and brown colors for the two wavelengths. For clarity, the data of the sensor chips before APTES functionalization (bare chip) is not shown. The final refractive index and thickness obtained with this method were 1.41, and 1.7 nm.

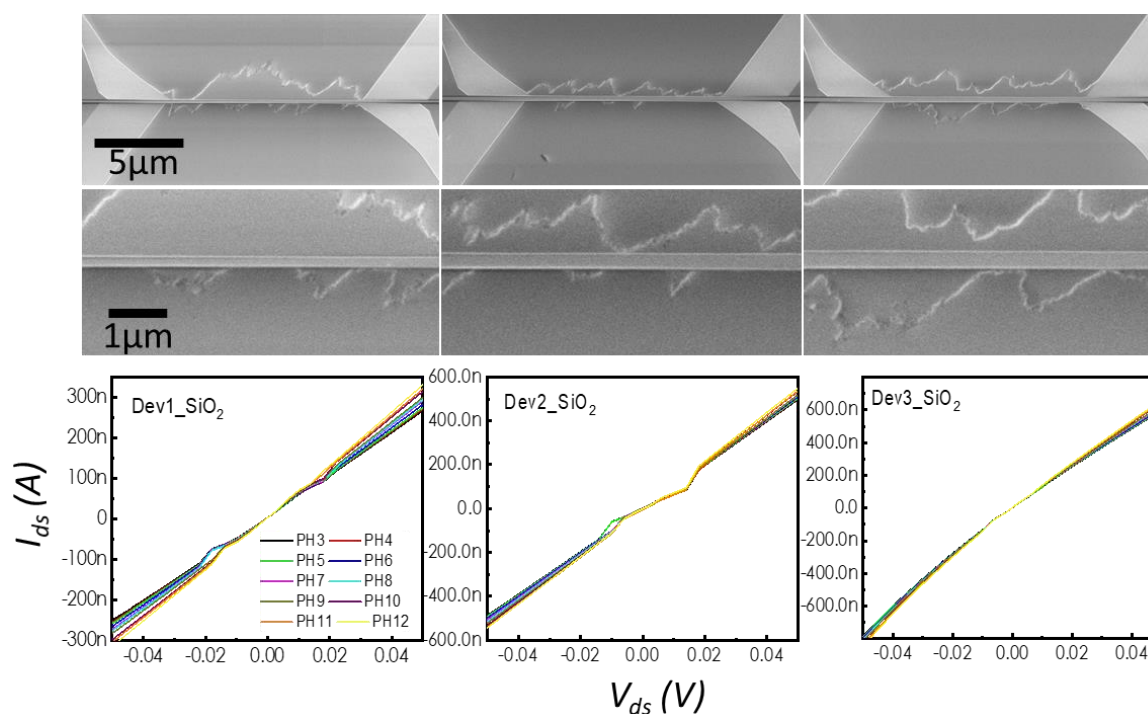


**Figure S2.** SEM pictures and the corresponding  $I_{ds}$  vs  $V_{ds}$  pH curves from devices 1 to 3.

## 2. pH sensitivity of FinFET devices

Figure S1 2 reports SEM pictures of devices 1 to 3 with channel widths of 190, 300 and 320 nm respectively, and their corresponding pH response of the output characteristics. Device 2 and 3 showed higher currents and lower current sensitivity ( $\Delta I/I$ ) than device 1 owing to their bigger width.

Figure S1 3 shows the change in  $V_{GS}$  vs. buffer pH from the devices 1 to 3 (using squares, circles and triangles, respectively) measured before ( $\text{SiO}_2$ ) and after the APTES silanization process (represented in black and red colours respectively). The individual  $V_{GS}$  values for different buffer pH were evaluated by fixing the  $I_{ds}$  in the transfer characteristics and

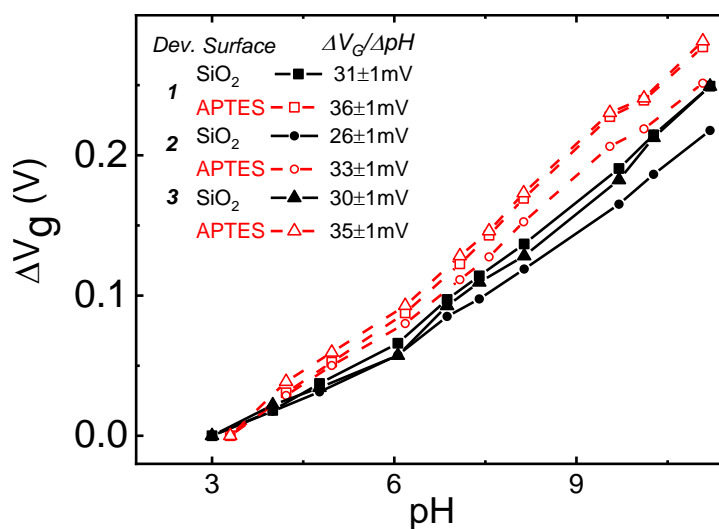


**Figure S3.** Plot showing the variation of  $V_{GS}$  change extracted from the transfer characteristics as a function of buffer pH for 3 FinFETs (Ch1, 2,3) measured before ( $\text{SiO}_2$ ) and after the APTES silanization. The  $V_{GS}$  change was extracted by subtracting the  $V_{GS}$  values obtained after fixing the  $I_{ds}$ , at each buffer pH value with respect to the value at pH 3.

were subtracted with  $V_{GS}$  for pH 3 to determine  $V_{GS}$  change. As can be interpreted from the plot, the variation of  $V_{GS}$  with buffer pH and pH sensitivity was comparable in all devices.

### 3. Ellipsometry calculations

We measured the thickness of APTES on silanized SiO<sub>2</sub>/Si chips *via* ellipsometry technique in order to compare it with the SPR data. Conventional Si chips with a thin layer of SiO<sub>2</sub> (5 nm) were silanized using vapour-phase method as described in the main text and characterized using ellipsometry before and after the silanization process. We fitted the data using Cauchy's model as described earlier by Munief et al. and obtained thickness of 1.9±0.2 nm [2].

### 4. Comparison of experimental $\beta_{int}$

Figure SI-4 shows the comparison between the experimental buffering capacitance ( $\beta_{int}$ ) obtained from the variations of the surface potential of SiO<sub>2</sub> (in a) and the APTES functionalised surface (in b) in device 1. The data were obtained using equations 3, 4, and 5 from the main text. While  $\beta_{int}$  for SiO<sub>2</sub> only has one peak corresponding to the protonation of silanol groups, for APTES it has additional peaks corresponding to the protonation and deprotonation of amino groups.

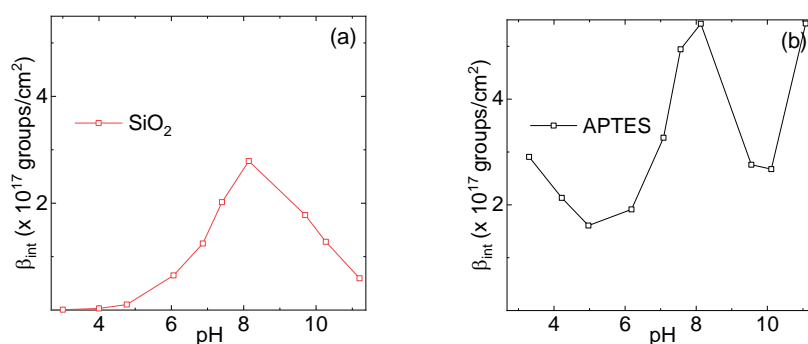


**Figure S4.** comparison between the buffering capacitance of SiO<sub>2</sub> (a) and the APTES functionalised surface in device 1.

### References:

1. Kari, O.K., Rojalín, T., Salmaso, S., Barattin, M., Jarva, H., Meri, S., Yliperttula, M., Viitala, T. and Urtti, A., Multi-parametric surface plasmon resonance platform for studying liposome-serum interactions and protein corona formation. *Drug Deliv. Transl. Res.* **2017**, *7*, 228–240.
2. Munief, W.M., Heib, F., Hempel, F., Lu, X., Schwartz, M., Pachauri, V., Hempelmann, R., Schmitt, M. and Ingebrandt, S. silane deposition via gas-phase evaporation and high-resolution surface characterization of the ultrathin siloxane coatings. *Langmuir* **2018**, *34*, 10217–10229.